

Topological Phase Transition in an Archetypal f -electron Correlated System: Ce

Junwon Kim^{1,*}, Dongchoon Ryu^{1,*}, Chang-Jong Kang^{1,†}, Kyoo Kim^{1,2}, Hongchul Choi^{1,‡}, T.-S. Nam¹, and B. I. Min^{1§}

¹Department of Physics,

Pohang University of Science and Technology,
Pohang 37673, Korea

²MPPHC_CPM, Pohang University of Science and Technology,
Pohang 37673, Korea

(Dated: October 5, 2021)

A typical f -electron Kondo lattice system Ce exhibits the well-known isostructural transition, the so-called γ - α transition, accompanied by an enormous volume collapse. Most interestingly, we have discovered that a topological-phase transition also takes place in elemental Ce, concurrently with the γ - α transition. Based on the dynamical mean-field theory approach combined with density functional theory, we have unravelled that the non-trivial topology in α -Ce is driven by the f - d band inversion, which arises from the formation of coherent $4f$ band around the Fermi level. We captured the formation of the $4f$ quasi-particle band that is responsible for the Lifshitz transition and the non-trivial Z_2 topology establishment across the phase boundary. This discovery provides a concept of “topology switch” for topological Kondo systems. The “on” and “off” switching knob in Ce is versatile in a sense that it is controlled by available pressure (~ 1 GPa) at room temperature.

Physics of strongly-correlated f -electron materials has been a longstanding subject of special interest due to complex interplay among the underlying interactions, such as strong Coulomb correlation, spin-orbit (SO) coupling, and the hybridization of the localized f and conduction electrons. More intriguing is that the interplay is very sensitive to small changes in the external parameters. Elemental Ce, which has one occupied f electron in its atomic phase, is a prototypical f -electron Kondo lattice system exhibiting such sensitivity. Indeed Ce shows a rich phase diagram (see Fig. 1) and many interesting physical properties as a function of temperature (T) and pressure (P) [1–4]. The first-order isostructural volume-collapse transition from γ to α phase of face-centered cubic (fcc) Ce is the most representative phenomenon that experiences the sensitivity. However, the driving mechanism of the γ - α transition is still under debate, between the two well-known models: Mott transition [5] vs. Kondo volume collapse [6]. The current consensus is that there exists at least a significant change in the Kondo hybridization between the localized $4f$ electrons and conducting electrons across the transition [7–10]. This peculiarity in Ce could facilitate the emergence of nontrivial topology in the ground-state α -phase of Ce.

In a recent theoretical work on topological Kondo insulator [11], it is shown that the Kondo hybridization in f -electron systems can play an important role in the formation of non-trivial topology. Since then, many subsequent studies have been reported to search for non-trivial topological materials, where the Kondo hybridization gap exists, *e.g.*, CeNiSn, CeRu₄Sn₆, Ce₃Bi₄Pt₃, SmB₆, SmS, and YbB₁₂ [11–17]. Despite extensive studies, however, the topological nature of mother elements, Ce, Sm, and Yb, supplying the correlated f -electrons to the above Kondo insulator compounds, has not been explored yet. Here we report, based on the dynamical

mean-field theory (DMFT) approach combined with density functional theory (DFT) that has been successful to describe electronic structures of Ce and Ce compounds [8, 9, 18, 19], that a narrow f -band metal α -Ce has the non-trivial topology of topological-insulator (TI)-type and topological-crystalline-insulator (TCI)-type nature, and the topological phase transition and the Lifshitz electronic transition occur concomitantly with the γ - α volume collapse transition in Ce.

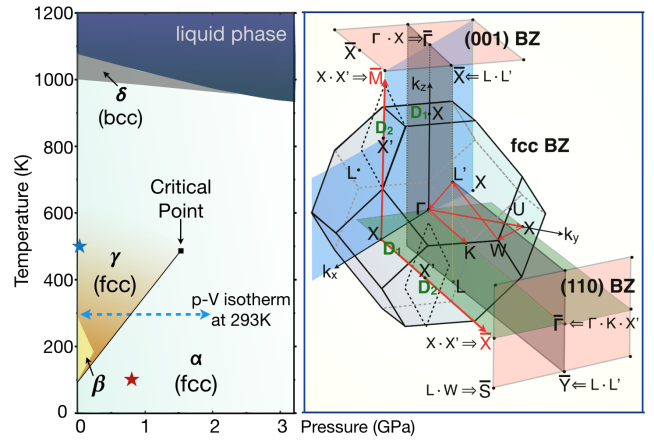


FIG. 1: (Left) A phase diagram of Ce [20] (see also the supplement [21]). α -Ce at “red star” and γ -Ce at “blue star” are selected for the comparison of electronic structures in Fig. 2. The blue-dotted line corresponds to the P - V isotherm at 293 K. (Right) The bulk BZ of fcc Ce and its (001) and (110) surface BZ. There are two independent mirror planes of $k_y = 0$ (in blue) and $k_x = k_y$ (in gray), which, respectively, yield two mirror-symmetry lines along M - $\bar{\Gamma}$ - \bar{M} and \bar{X} - $\bar{\Gamma}$ - \bar{X} in the (001) surface BZ. Similarly, in the (110) surface BZ, two mirror-symmetry lines are formed along \bar{Y} - $\bar{\Gamma}$ - \bar{Y} and \bar{X} - $\bar{\Gamma}$ - \bar{X} .

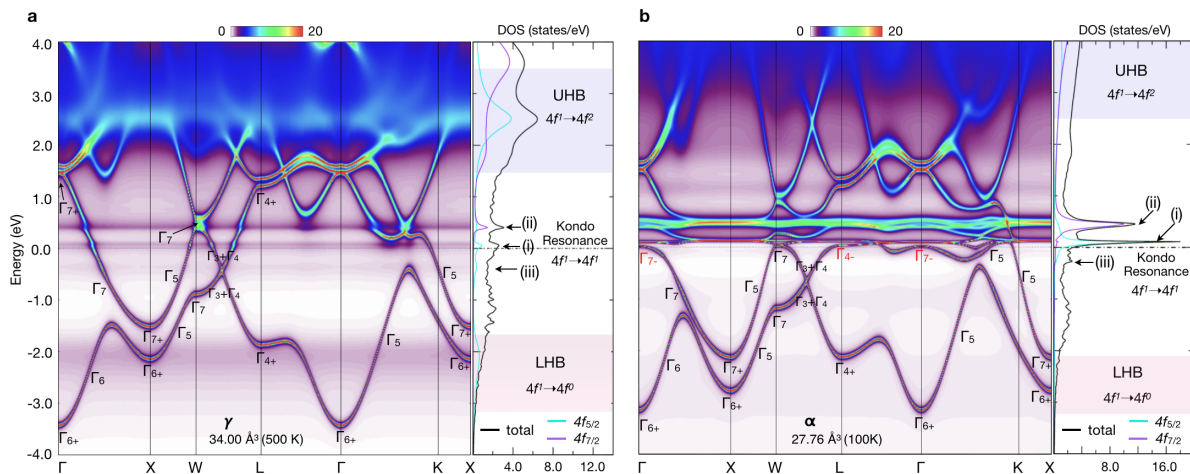


FIG. 2: (a) The DMFT electronic structure and DOS for γ -Ce calculated at $V = 34 \text{ \AA}^3$ ($P = \text{ambient pressure}$) and $T = 500 \text{ K}$, and (b) those for α -Ce calculated at $V = 27.76 \text{ \AA}^3$ ($P = 0.88 \text{ GPa}$) and $T = 100 \text{ K}$. The $4f$ spectral weights of both phases consist of mainly three parts: UHB at $2 \sim 4 \text{ eV}$, LHB at $-2.0 \sim -2.5 \text{ eV}$, and the Kondo resonance near E_F . In addition to the Kondo resonance near E_F (i), the SO side peaks (ii), (iii) are seen at $\sim \pm 0.3 \text{ eV}$. Note that only α -Ce shows the coherent quasi-particle $4f$ band around E_F , which is shown more clearly in Fig. 3.

Figure 2 shows the DMFT band structures and the densities of states (DOSs) of γ - and α -Ce. In the DMFT calculations, we have used the Coulomb correlation (U) and the exchange (J) interaction parameters of $U = 5.5 \text{ eV}$ and $J = 0.68 \text{ eV}$ for the Ce f -electrons (refer to the supplement for the computational details) [21]. The $4f$ spectral weights of both phases have three main parts in common: the lower Hubbard band (LHB) at $-2.0 \sim -2.5 \text{ eV}$ corresponding to the $4f^0$ final state, the upper Hubbard band (UHB) at $2 \sim 4 \text{ eV}$ corresponding to the $4f^2$ final state, and the Kondo resonances near the Fermi level (E_F) corresponding to the $4f^1$ final states. The energy positions of LHB and UHB are in good agreement with photoemission spectroscopy (PES) [22–24] and inverse PES experiments [26]. One of the most notable features in Fig. 2 is that the spectral weight of the Kondo resonance around E_F is much stronger in α -Ce than in γ -Ce, and exhibits the coherent quasi-particle band feature in α -Ce, as is consistent with previous PES [22–26] and theoretical reports [27–30]. As will be discussed below, these contrasting Kondo-resonance features between the two phases lead to the quite different topological classes: trivial and non-trivial Z_2 topologies for γ -Ce and α -Ce, respectively.

The incoherent and coherent $4f$ spectral weights for γ -Ce and α -Ce, respectively, are more clearly shown in the amplified DMFT band structures in Fig. 3. It is seen in Fig. 3a that, for γ -Ce, $4f$ electrons are incoherent, and so mainly the $5d$ band crosses E_F , which agrees well with the optical spectroscopy result [31]. In contrast, for α -Ce, the coherent $4f$ quasi-particle band feature is evident near E_F in Fig. 3b, which is the origin of the effective-mass enhancement of charge carriers and the change of

the charge carrier character from $5d$ to $4f$. The coherent band feature for α -Ce is corroborated by the fact that the DMFT bands have almost the same dispersion as the renormalized DFT bands rescaled approximately by $1/2$ (dotted green-line in Fig. 3b).

The different electronic structures between the two phases are also reflected in the Fermi surfaces (FSs). The shapes of FSs in Fig. 3d are topologically different, suggesting that γ - α transition corresponds to the Lifshitz transition (see the supplement) [21]. It is noteworthy in Fig. 3d that, while the DMFT FS of γ -Ce is very close to that obtained from the DFT-opencore (“ $4f$ -opencore”) calculation considering the $4f$ electrons as core electrons, the DMFT FS of α -Ce is quite similar to the DFT FS. These results indicate that, for γ -Ce, the contribution of $4f$ electrons to the FS is negligible, and, for α -Ce, the $4f$ quasi-particle band at E_F can be described properly by the DFT band (see Fig. S1 of the supplement) [21].

The key ingredient that makes the difference has something to do with the degree of the renormalization factor (quasi-particle weight) Z , arising from the Coulomb correlation interaction of $4f$ electrons. The renormalization factor Z is obtained from the slope of the real-part of the self-energy $\Sigma(\omega)$ at E_F . As shown Fig. S4 of the supplement [21], we have obtained qualitatively different behaviors of $\Sigma(\omega)$ ’s between the α and γ phases, which produce quite distinct electronic structures and resulting physical parameters. Indeed, Fig. 3e shows that Z increases discontinuously across the γ - α transition. As a result, both the hybridization strength $\Delta(\omega)$ (Fig. 3c) and the f - f hopping strength, which are to be effectively proportional to Z , are enhanced for α -Ce, which give rise to the enhanced $4f$ spectral weight and help to form the

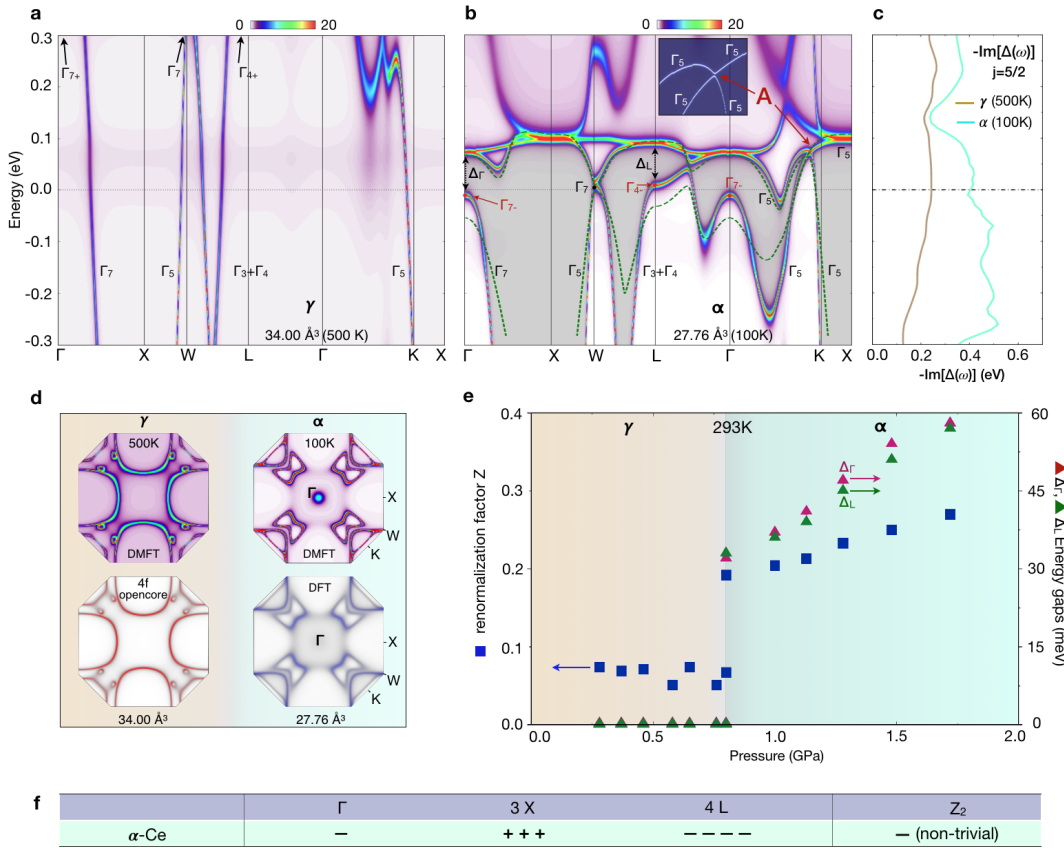


FIG. 3: The amplified DMFT electronic structures near E_F : (a) for γ -Ce and (b) for α -Ce. For γ -Ce, $4f$ states are hardly seen, because they are incoherent. For α -Ce, the coherent $4f$ bands formed around E_F produce, via the hybridization with the conduction band, the separated bands with the gap in-between (colored in gray). There exist clear energy gaps at the TRIM points of Γ , X and L , and also small energy gaps at W , in-between L - Γ , and at “A” along Γ - K . The inset shows the gap formation at “A”, arising from the same Γ_5 symmetry of the crossing bands [32]. The green-dotted lines overlaid with DMFT bands are the DFT bands rescaled by 1/2. (c) Imaginary part of the DMFT hybridization function $\Delta(\omega)$. (d) DMFT and DFT FSs for both phases (see also Fig. S1 [21]). (e) The renormalization factor Z and the energy gaps at Γ and L (Δ_Γ and Δ_L) are displayed as a function of pressure (see also Figs. S2-S4 [21]). The first-order-type phase transition is manifested across the γ - α transition. (f) The product of the parity eigenvalues of α -Ce at 8 TRIM points in the fcc BZ.

coherent $4f$ band around E_F [29].

The evolution of the electronic structure across the γ - α transition makes the elemental Ce more interesting in a topological sense. The coherent quasi-particle band in α -Ce, which, via the hybridization with the conduction band, brings about the hybridization gap in the α -Ce phase, as indicated by gray-shaded area in Fig. 3b. The energy gaps are clearly seen at every time-reversal invariant momentum (TRIM) points of Γ , X , and L , while those at W and in-between L - Γ are barely gapped. Then, with respect to the hybridization gap, the $5d$ band of even parity and the $4f$ band of odd parity are inverted at the TRIM point X . Since the crystal structure is symmetric under the inversion operation, the additional odd parity to the TRIM points yields the non-trivial Z_2 topology of α -Ce, as shown in Fig. 3f.

Figure 3e shows that the non-trivial Z_2 topology in α -

Ce is established at the very starting edge (volume 28 \AA^3 at 293 K) of α -phase in the γ - α transition. Note that no gaps are present in the γ phase, but the gaps at the TRIM points, Δ_Γ and Δ_L of about 30 meV ($\Delta_X > 2 \text{ eV}$), are suddenly developed in the α phase. This implies that the topological phase transition would occur concomitantly with the γ to α volume collapse transition. The more detailed evolution of the band structures across the γ - α transition is given along a P - V isotherm at 293 K in Fig. S2 of the supplement [21].

In order to confirm the non-trivial Z_2 topological invariance of α -Ce, we have performed the surface electronic structure calculations for the slab geometry of α -Ce with (001) surface and explored the existence of topological surface states (TSSs) in Fig. 4a. Note that, as shown in Fig. 1, one X point is projected onto $\bar{\Gamma}$, while two non-equivalent X and X' are projected onto \bar{M} of

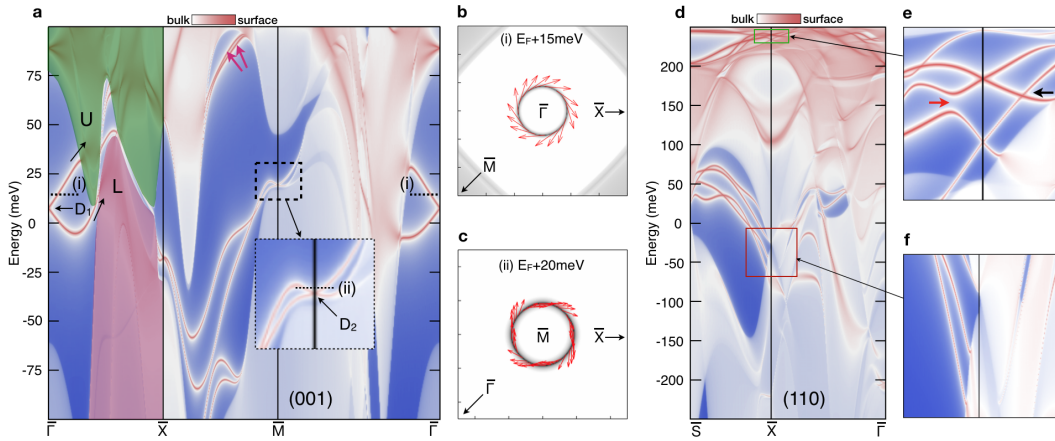


FIG. 4: (Color online) **(a)** The (001) surface electronic structure of α -Ce, calculated by the tight-binding (TB) model with semi-infinite slabs. The TB Hamiltonian is constructed from the DFT band result (rescaled by 1/2 near E_F). **(b),(c)** The helical spin structures of the “D₁” and “D₂” Dirac-cone energy surfaces, as indicated by (i) and (ii), respectively. **(d)** The (110) surface electronic structure of α -Ce. **(e),(f)** Amplified band structures inside the green-square and the red-square, respectively, in (D). In (E), TSSs of a typical TCI-type nature are revealed with the gapped (red arrow) and protected (black arrow) Dirac points, while, in (F), TSSs are mostly buried under the bulk-projected bands.

the (001) surface BZ. Indeed, as shown in Fig. 4a, the TSSs and corresponding Dirac points emerge in the indirect gap region at $\bar{\Gamma}$ (“D₁”) and \bar{M} (“D₂”). Due to the bulk metallic nature of α -Ce, most part of the Dirac bands at \bar{M} is buried under the bulk-projected bands and so the band connectivity is not clear. Nevertheless, it is evident in Fig. 4a that the surface states along $\bar{\Gamma}$ - \bar{X} are the Dirac-cone states, because the lower surface band reaches the violet-colored band (“L”) below the indirect gap, while the upper one reaches the green-colored band (“U”) above the indirect gap. The helical spin texture of the corresponding Dirac cone FS around $\bar{\Gamma}$ and \bar{M} in Fig. 4b and 4c also manifests the spin-momentum locking behavior, reflecting its topological nature.

The double Dirac points, which are supposed to be at \bar{M} due to the projection of two non-equivalent X TRIM points (Fig. 1), are to be separated due to the hybridization between the bands of the double Dirac cones. On the (001) surface Brillouin-Zone (BZ) of α -Ce, there are two mirror symmetric lines, $\bar{\Gamma}$ - \bar{X} and $\bar{\Gamma}$ - \bar{M} , as shown in Fig. 1, which could play a key role in realizing the TCI-type nature. It is thus obvious that the band crossing along \bar{X} - \bar{M} that is not a mirror symmetric line would be gapped, but that along \bar{M} - $\bar{\Gamma}$ needs further consideration. However, the surface states along \bar{M} - $\bar{\Gamma}$ are completely buried under the bulk projected bands, and so it is not easy to identify the specific TCI-type band feature in Fig. 4a. In view of the surface states inside the dotted-black square and those along \bar{X} - \bar{M} designated by red arrows in Fig. 4a, we just conjecture that the band crossing along \bar{M} - $\bar{\Gamma}$ would be gapped to have Rashba-type surface states, as reported for the golden phase of SmS (g -SmS) that is expected to have the same topological symmetry

as α -Ce [33]. In fact, α -Ce is found to have the same mirror Chern numbers as g -SmS [34], as shown in Fig. S5 of the supplement [21].

We have also examined the TSSs for the (110) and (111) surfaces of α -Ce. For the (110) surface, single and double Dirac points are expected to be located at $\bar{\Gamma}$ and \bar{X} , respectively, as shown in Fig. 1. For the (111) surface, only the single Dirac point is expected at \bar{M} , as shown in Fig. S6 of the supplement [21]. As shown in Fig. 4d and Fig. S6, however, neither (110) nor (111) surface states show a clear TI-type or TCI-type signature in the hybridization gap region, because, here too, most of the surface states near E_F are buried under the bulk-projected bands. In this circumstance, for the (110) surface, one apparent TCI signature is seen at \bar{X} near 240 meV in Fig. 4e, which demonstrated the gapped and protected Dirac points along \bar{X} - \bar{S} (red arrow) and \bar{X} - $\bar{\Gamma}$ (black arrow), respectively. This suggests that the near- E_F TSSs buried under the bulk-projected bands in Fig. 4f would also have the TCI-type band nature.

Our finding highlights that a typical narrow f -band metal α -Ce is a topological Kondo system of TI- and TCI-type nature, and the “on” and “off” topology switch can be operative by using a P -tuning or T -tuning knob, accompanied by the first-order volume-collapse and Lifshitz transitions. So Ce would be an excellent test-bed for investigating the topological phase transition in f -electron Kondo lattice systems. It is thus highly desirable to explore the topological surface states in α -Ce, preferentially for its (001) surface, by using high resolution angle-resolved PES measurement.

Acknowledgments— We would like to thank J.D. Denlinger, J.-S. Kang, and J.H. Shim for

helpful discussions. This work was supported by the NRF (Grant No. 2017R1A2B4005175, Grant No. 2018R1A6A3A01013431, Grant No. 2016R1D1A1B02008461), Max-Planck POSTECH/KOREA Research Initiative (No. 2016K1A4A4A01922028), the POSTECH BSRI Grant, and the KISTI supercomputing center (Grant No. KSC-2017-C3-0057).

* Co-first authors: They contributed equally.

† Present address: Department of Physics and Astronomy, Rutgers University, Piscataway, New Jersey, 08854, USA

‡ Present address: Scuola Internazionale Superiore di Studi Avanzati Trieste 34136, Italy

§ e-mail: bimin@postech.ac.kr

- [1] D. Koskenmaki, and K. A. Gschneidner, *Handbook on the Physics and Chemistry of Rare Earths Ch. 4* (Elsevier, Amsterdam, 1978)
- [2] J. C. Lashley, A. C. Lawson, J. C. Cooley, B. Mihaila, C. P. Opeil, L. Pham, W. L. Hults, J. L. Smith, G. M. Schmiedeshoff and F. R. Drymiotis, Tricritical Phenomena at the $\gamma \rightarrow \alpha$ Transition in $\text{Ce}_{0.9-x}\text{La}_x\text{Th}_{0.1}$ Alloys. *Phys. Rev. Lett.* **97**, 235701 (2006).
- [3] N. Lanata, Yong-Xin Yao, Cai-Zhuang Wang, Kai-Ming Ho, J. Schmalian, K. Haule and G. Kotliar, γ - α Isostructural Transition in Cerium. *Phys. Rev. Lett.* **111**, 196801 (2013).
- [4] J. Wittig, Superconductivity of Cerium Under Pressure. *Phys. Rev. Lett.* **21**, 1250 (1968).
- [5] B. Johansson, The α - γ transition in cerium is a Mott transition. *Philos. Mag.* **30**, 469 (1974).
- [6] J. W. Allen and R. M. Martin, Kondo Volume Collapse and the $\gamma \rightarrow \alpha$ Transition in Cerium. *Phys. Rev. Lett.* **49**, 1106 (1982).
- [7] A. P. Murani, Magnetic Form Factor of α -Ce: Towards Understanding the Magnetism of Cerium. *Phys. Rev. Lett.* **95**, 256403 (2005).
- [8] B. Chakrabarti, M. E. Pezzoli, G. Sordi, K. Haule and G. Kotliar, α - γ transition in cerium: Magnetic form factor and dynamic magnetic susceptibility in dynamical mean-field theory. *Phys. Rev. B* **89**, 125113 (2014).
- [9] K. Haule, V. Oudovenko, S. Y. Savrasov and G. Kotliar, The $\alpha \rightarrow \gamma$ Transition in Ce: A Theoretical View from Optical Spectroscopy. *Phys. Rev. Lett.* **94**, 036401 (2005).
- [10] K. Haule and T. Birol, Free Energy from Stationary Implementation of the DFT+ DMFT Functional. *Phys. Rev. Lett.* **115**, 256402 (2015).
- [11] M. Dzero, K. Sun, V. Galitski and P. Coleman, Topological Kondo Insulators. *Phys. Rev. Lett.* **104**, 106408 (2010).
- [12] M. Sundermann, F. Strigari, T. Willers, H. Winkler, A. Prokofiev, J.M. Ablett, J.P. Rueff, D. Schmitz, E. Weschke, M. Moretti Sala, A. Al-Zein, A. Tanaka, M.W. Haverkort, D. Kasinathan, L.H. Tjeng, S. Paschen and A. Severing, CeRu_4Sn_6 : a strongly correlated material with nontrivial topology. *Sci. Rep.* **5**, 17937 (2015).
- [13] N. Wakeham, P. F. S. Rosa, Y. Q. Wang, M. Kang, Z. Fisk, F. Ronning and J. D. Thompson, Low-temperature conducting state in two candidate topological Kondo insulators: SmB_6 and $\text{Ce}_3\text{Bi}_4\text{Pt}_3$. *Phys. Rev. B* **94**, 035127 (2016).
- [14] F. Lu, J. Z. Zhao, H. Weng, Z. Fang and X. Dai, *Phys. Rev. Lett.* **110**, 096401 (2013).
- [15] M. Neupane, N. Alidoust, S.Y. Xu, T. Kondo, Y. Ishida, D.J. Kim, C. Liu, I. Belopolski, Y.J. Jo, T.R. Chang, H.T. Jeng, T. Durakiewicz, L. Balicas, H. Lin, A. Bansil and S. Shin, Surface electronic structure of the topological Kondo-insulator candidate correlated electron system SmB_6 . *Nat. Commun.* **4**, 2991 (2013).
- [16] Z. Li, J. Li, P. Blaha and N. Kioussis, Predicted topological phase transition in the SmS Kondo insulator under pressure. *Phys. Rev. B* **89**, 121117(R) (2014).
- [17] K. Hagiwara, Y. Ohtsubo, M. Matsunami, S. Ideta, K. Tanaka, H. Miyazaki, J. E. Rault, P. L. Fèvre, F. Bertran, A. Taleb-Ibrahimi, R. Yukawa, M. Kobayashi, K. Horiba, H. Kumigashira, K. Sumida, T. Okuda, F. Iga and S. Kimura, Surface Kondo effect and non-trivial metallic state of the Kondo insulator YbB_{12} . *Nat. Commun.* **7**, 12690 (2016).
- [18] J. H. Shim, K. Haule and G. Kotliar, Modeling the localized-to-itinerant electronic transition in the heavy fermion system CeIrIn_5 . *Science* **318**, 1615 (2007).
- [19] E. A. Goremychkin, H. Park, R. Osborn, S. Rosenkranz, J.-P. Castellán, V. R. Fanelli, A. D. Christianson, M. B. Stone, E. D. Bauer, K. J. McClellan, D. D. Byler and J. M. Lawrence, Coherent band excitations in CePd_3 : A comparison of neutron scattering and *ab initio* theory. *Science* **359**, 186 (2018).
- [20] M. J. Lipp, D. Jackson, H. Cynn, C. Aracne, W. J. Evans and A. K. McMahan, Thermal Signatures of the Kondo Volume Collapse in Cerium. *Phys. Rev. Lett.* **101**, 165703 (2008).
- [21] See the Supplementary Material for (i) computational details, (ii) phase boundaries, (iii) Lifshitz transition, (iv) pressure-dependent DMFT physical quantities, (v) TCI-type nature, and (vi) surface states at (111) surface of Ce.
- [22] D. M. Wieliczka, C. G. Olson and D. W. Lynch, High-resolution photoemission study of γ - and α -cerium. *Phys. Rev. B* **29**, 3028 (1984).
- [23] F. Patthey, B. Delley, W.-D. Schneider and Y. Baer, Low-Energy Excitations in α - and γ -Ce Observed by Photoemission. *Phys. Rev. Lett.* **55**, 1518 (1985).
- [24] E. Weschke, C. Laubschat, T. Simmons, M. Domke, O. Strebel and G. Kaindl, Surface and bulk electronic structure of Ce metal studied by high-resolution resonant photoemission. *Phys. Rev. B* **44**, 8304 (1991).
- [25] Q. Y. Chen, W. Feng, D. H. Xie, X. C. Lai, X. G. Zhu and L. Huang, Localized to itinerant transition of f electrons in ordered Ce films on $\text{W}(110)$, *Phys. Rev. B* **97**, 155155 (2018).
- [26] M. Grioni, P. Weibel, D. Malterre and Y. Baer, Resonant inverse photoemission in cerium-based materials. *Phys. Rev. B* **55**, 2056 (1997).
- [27] M. B. Zöflf, I. A. Nekrasov, Th. Pruschke, V. I. Anisimov and J. Keller, Spectral and Magnetic Properties of α - and γ -Ce from Dynamical Mean-Field Theory and Local Density Approximation. *Phys. Rev. Lett.* **87**, 276403 (2001).
- [28] K. Held, A. K. McMahan and R. T. Scalettar, Cerium Volume Collapse: Results from the Merger of Dynamical Mean-Field Theory and Local Density Approximation. *Phys. Rev. Lett.* **87**, 276404 (2001).

- [29] B. Amadon and A. Gerossier, Comparative analysis of models for the α - γ phase transition in cerium: A DFT+DMFT study using Wannier orbitals *Phys. Rev. B* **91**, 161103(R) (2015).
- [30] L. Huang and H. Lu, Electronic structure of cerium: A comprehensive first-principles study. *Phys. Rev. B* **99**, 045122 (2019).
- [31] J. W. van der Eb, A. B. Kuzmenko and D. van der Marel, Infrared and Optical Spectroscopy of α - and γ -Phase Cerium. *Phys. Rev. Lett.* **86**, 3407 (2001).
- [32] Here, to capture the quasi-particle feature, the imaginary part of self-energy ($\text{Im}\Sigma(\omega)$) is set to be zero, namely, the Hamiltonian is assumed to be Hermitian.
- [33] C.-J. Kang, H. C. Choi, K. Kim and B. I. Min, Topological Properties and the Dynamical Crossover from Mixed-Valence to Kondo-Lattice Behavior in the Golden Phase of SmS. *Phys. Rev. Lett.* **114**, 166404 (2015).
- [34] C.-J. Kang *et al.*, Unpublished (2019).

Supplement of “Topological Phase Transition in an Archetypal f -electron Correlated System: Ce”

Junwon Kim^{1,*}, Dongchun Ryu^{1,*}, Chang-Jong Kang^{1,†}, Kyoo Kim^{1,2}, Hongchul Choi^{1,‡}, T.-S. Nam¹, and B. I. Min^{1§}

¹*Department of Physics,
Pohang University of Science and Technology,
Pohang 37673, Korea*

²*MPPHC-CPM, Pohang University of Science and Technology,
Pohang 37673, Korea*

I. COMPUTATIONAL DETAILS

DFT+DMFT: To describe the topological phase transition across the γ - α transition, it is important to have accurate band structures of both α and γ phases since the band structures give the information on which phase might have the non-trivial Z_2 topology. Most of all, the correlation effect should carefully be considered since Ce $4f$ electrons are spatially much localized. To consider the correlation effect properly, we have used the charge self-consistent DFT+DMFT scheme [1] implemented in the full-potential code of WIEN2k [2].

In the actual DMFT problem, the solution of the auxiliary quantum impurity problem is achieved by the continuous time quantum Monte Carlo (CTQMC) solver [3, 4]. For the double-counting functional, we used the nominal double-counting scheme introduced in Ref. [5, 6]. The on-site Coulomb correlation (U) and the exchange (J) interaction parameters were set by 5.5 eV and 0.68 eV, respectively, and the spin-orbit coupling is included.

Tight-binding model for surface states: From the comparison of DMFT and DFT band structures of α -Ce, we have found that the renormalized DFT band is useful to investigate the low-energy band structure, and so investigated the surface electronic structures of α -Ce, using the tight-binding (TB) model constructed from the renormalized DFT band result (rescaled by 1/2 at around EF). For the extraction of TB model parameters, the maximally localized Wannier functions were used [7–9]. Then we constructed the TB Hamiltonian employing the Wannier90 code [10] and performed semi-infinite TB slab calculations to obtain the surface states of α -Ce, using the Green function scheme [11] implemented in Wannier tools [12].

II. PHASE BOUNDARIES

Although some of the phase boundaries are still under debate due to the experimental uncertainty, it is generally accepted that there exist at least seven allotropic phases in solid Ce. In Fig. 1 of the text, fcc, bcc, and bct represent the face-centered cubic, body-centered cubic, and body-centered tetragonal structures, respectively. β -Ce has the double hexagonal-close packed (dhcp) structure. Among those phases, γ - α phase boundary is of great interest. The γ - α phase transition was discovered by Bridgman in 1927 [13]. But it became famous due to the isostructureness across the transition, which was observed in the x-ray experiment in 1940 [14], leading to a large volume decrease by 15% in its maximum. It is known that the size of isostructural volume collapse decreases as the temperature (T) increases, and finally disappears at a critical point (CP). According to recent high-quality X-ray diffraction data [15], the position of CP is located at the pressure (P) of 1.5 ± 0.1 GPa and $T = 480 \pm 10$ K. For the clear comparison of the electronic structures between α and γ phases, we chose two representative points, where both phases crystallize in face-centered cubic (fcc) structure with the space group of $Fm\bar{3}m$ (No.225), and α -Ce and γ -Ce have the lattice constants of 4.82 Å at $P = 0.81$ GPa and $T = 100$ K (“red star”) and 5.16 Å at the ambient pressure and $T = 500$ K (“blue star”) in Fig. 1, respectively [16, 17]. Both of them are relatively far from the CP.

*Co-first authors: They contributed equally.

†Present address: Department of Physics and Astronomy, Rutgers University, Piscataway, New Jersey, 08854, USA

‡Present address: Scuola Internazionale Superiore di Studi Avanzati Trieste 34136, Italy

§e-mail: bimin@postech.ac.kr

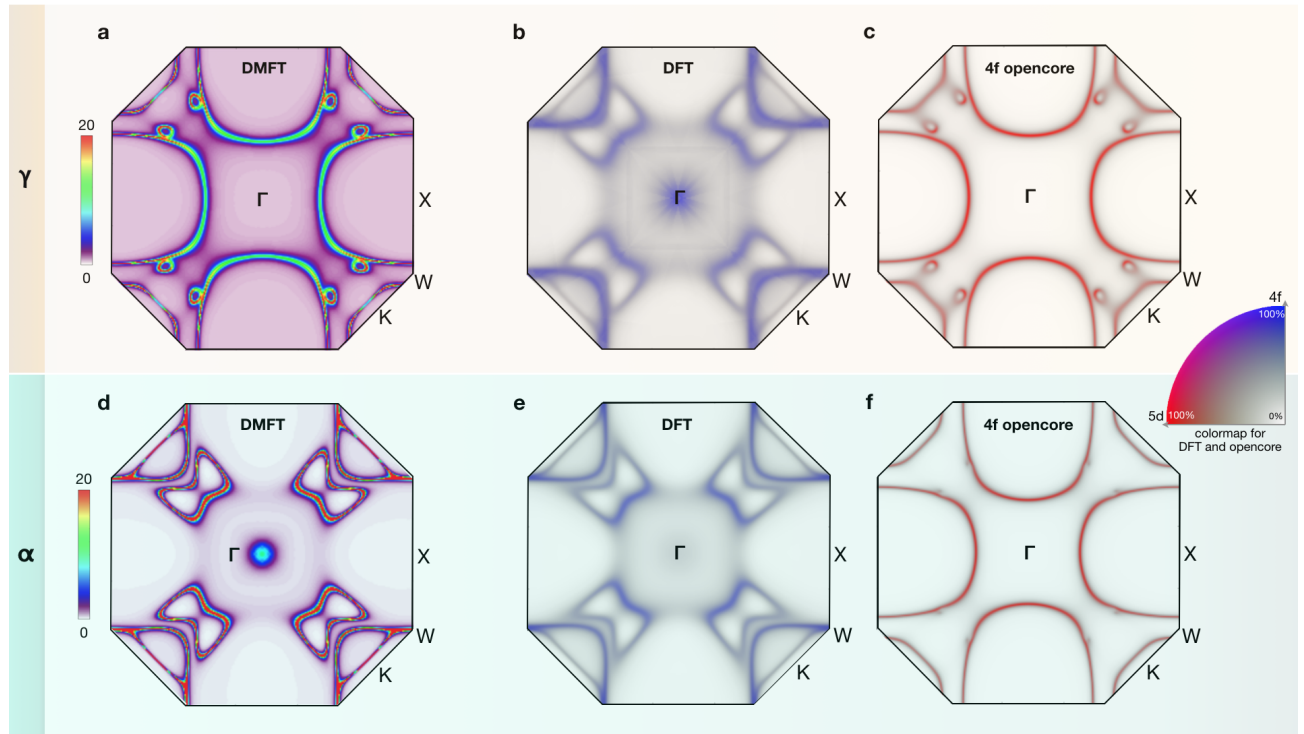


FIG. S1: **(a)-(c)** Fermi surfaces (FSs) of γ -Ce calculated at $T = 500$ K and $V = 34 \text{ \AA}^3$ by DMFT, DFT, and DFT-opencore (“4f-opencore”) methods, respectively. Note that the DMFT FS is very similar to the “4f-opencore” FS, which is composed of mostly $5d$ electrons. **(d)-(f)** FSs of α -Ce calculated at $T = 100$ K and $V = 27.76 \text{ \AA}^3$ by DMFT, DFT, and DFT-opencore (“4f-opencore”) methods, respectively. The DMFT FS shows a very good agreement with the DFT FS, which is composed of mostly $4f$ electrons. The seemingly blurred FSs from the DFT and DFT-opencore calculations originate just from the effect of the Gaussian broadening of each band.

III. LIFSHITZ TRANSITION ACROSS THE γ - α TRANSITION

In 1960, Lifshitz reported anomalies of thermodynamic and kinetic quantities due to an “electron transition” via the variation of the topology of Fermi surfaces [18]. Since γ - α phase transition happens in the absence of structural symmetry change, it is a good test material to observe the electron transition and corresponding anomalies in the thermodynamic and kinetic quantities. Interestingly, the size of isostructural volume collapse decreases as T increases. In Fig. S1, as an example of the Lifshitz transition, we have compared the Fermi surfaces (FSs) at two different volumes (i) $V = 34 \text{ \AA}^3$ ($T = 500$ K, ambient pressure) where γ phase is thermodynamically stable and (ii) $V = 27.76 \text{ \AA}^3$ ($T = 100$ K, $P = 0.88$ GPa) where α phase is thermodynamically stable, both of which are far from the phase boundary and the CP ($P = 1.5$ GPa). The FS topology in the low pressure ($V = 34 \text{ \AA}^3$) γ phase, which arises mostly from the delocalized $5d$ electrons, is transformed drastically into a new topology in the high pressure ($V = 27.76 \text{ \AA}^3$) α phase, as the coherent $4f$ band dominates the low energy spectrum. In the γ phase, the DMFT FS in Fig. S1a shows a very similar FS to that of “4f opencore” in Fig. S1c. Since the “4f opencore” calculation excludes the $4f$ electron in the valence state, the great similarity between the DMFT FS and the “4f opencore” FS implies that the $4f$ electrons in the γ phase have almost localized nature. On the other hand, in the α phase, the DMFT FS in Fig. S1d has a good agreement with the DFT FS in Fig. S1e, which indicates that the $4f$ electrons in the α phase behave as having a coherent quasi-particle band nature. The evolution from the localized to coherent band nature of $4f$ electrons is also shown in the volume-dependent band structures in Fig. S2 along the pressure-volume isotherm at a given $T = 293$ K.

Another interesting point is that Ce also shows a Lifshitz-type transition only by T change. A T -induced Lifshitz transition in the absence of a structural or magnetic phase transition is extremely rare in weakly correlated systems. This is because the electronic structure does not change much by T change. In strongly correlated systems, however, T could be one of the sources to drive the Lifshitz transition, as in the case of Ce, because the electronic structure becomes sensitive to the T change. Similar T -induced Lifshitz transitions were observed in the previous studies on CeIrIn₅ [19] and golden-phase SmS [20].

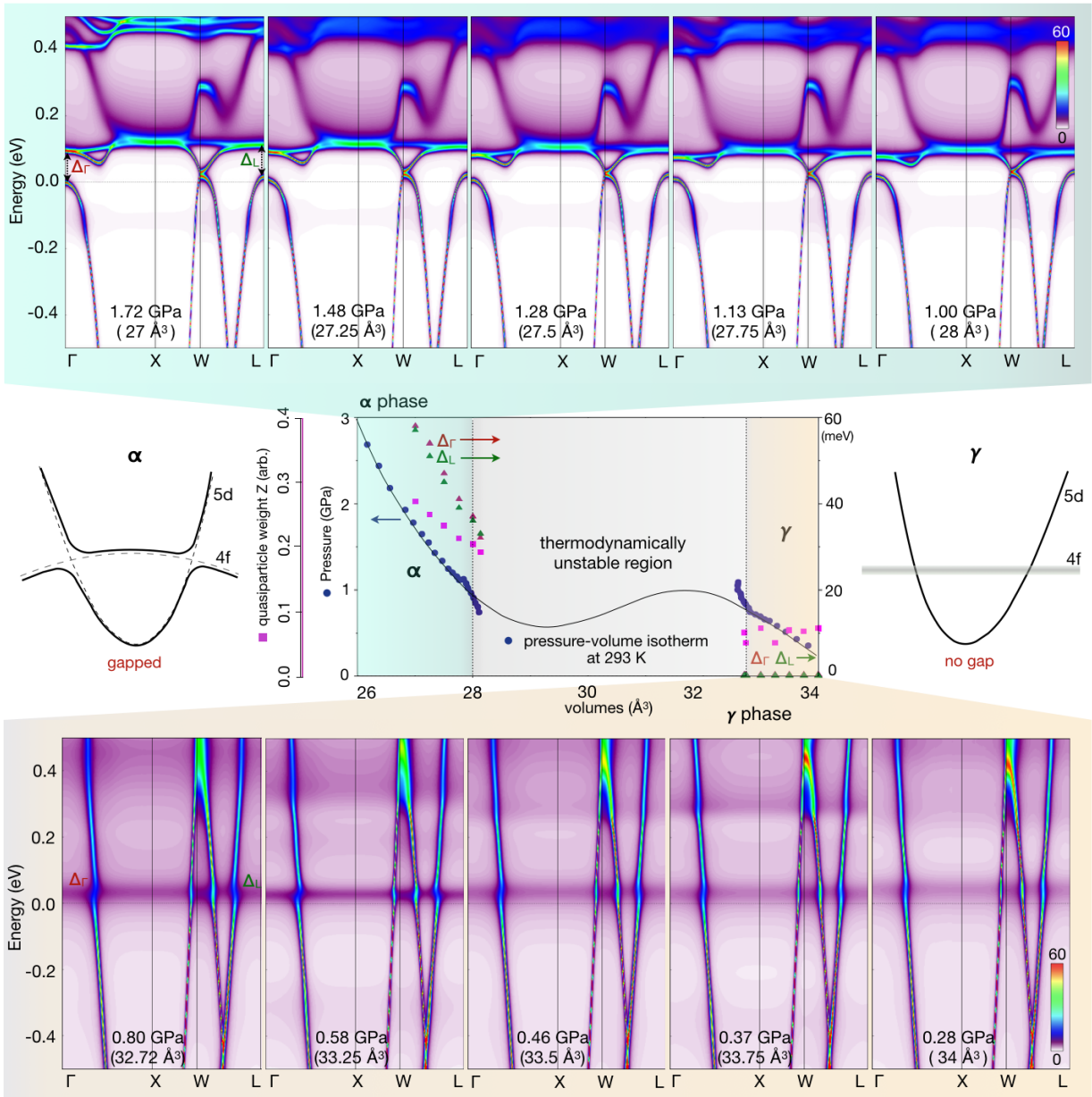


FIG. S2: (Color online) The pressure-volume isotherm at $T = 293$ K [15] and the evolution of gaps Δ_Γ and Δ_L at Γ and L as a function of volume. Maxwell construction is used to capture the end volume of the γ phase and the starting volume of the α phase, which correspond to about $V = 32.75$ Å³ and $V = 28$ Å³, respectively. At the very starting edge of the α phase, the gaps Δ_Γ and Δ_L become finite, in contrast to almost zero gap feature in the γ phase. The DMFT band structures as a function of volume are also displayed, which clearly shows the coherent $4f$ band formation for α -Ce with volume less than 28 Å³.

IV. PRESSURE-DEPENDENT EVOLUTIONS OF VARIOUS DMFT PHYSICAL QUANTITIES

Renormalization factor Z is displayed in Fig. S3(a) as a function of pressure. Since the DMFT f - f hopping strength and the DMFT f - d hybridization function $\Delta(\omega)$ are effectively proportional to the Z factor, the enhancement of Z factor helps the f electrons to form a quasi-particle band around E_F in the α -phase. Figure S3(B) shows that the total f electron occupation drops only slightly across the transition. But, as shown in Fig. S3(b) and (c), the abrupt reduction of f^1 probability accompanied by the abrupt enhancement of f^0 and f^2 probabilities indicates that f electrons in α -Ce become more or less delocalized. Figure S3(D)-(F) show the total and $4f$ DOS, the relaxation time τ , and the imaginary part of the DMFT hybridization function at E_F , $Im\Delta(0)$, across the γ - α transition. The

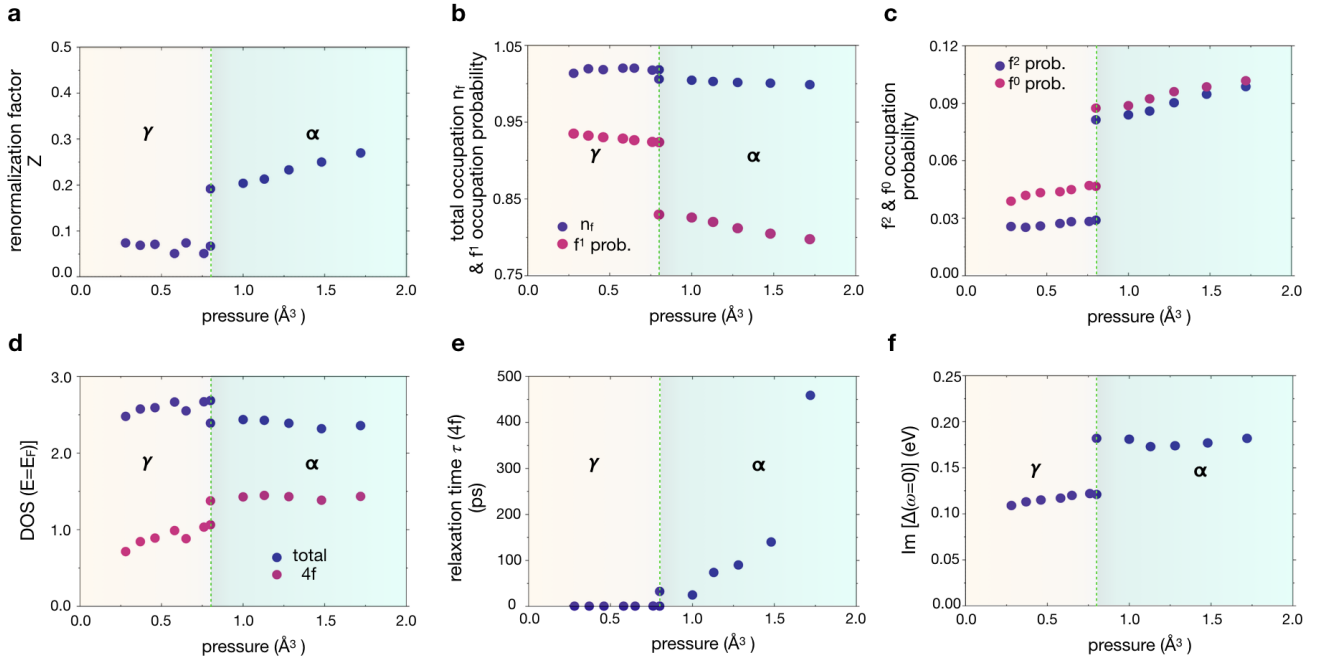


FIG. S3: (Color online) Pressure dependent DMFT physical parameters along the pressure-volume isotherm process at $T = 293\text{K}$. **(a)** Renormalization factor Z . **(b)** Occupation probabilities of f^0 and f^2 configurations. **(c)** Occupation of f -electrons, f^{tot} , and the occupation probability of f^1 configuration. **(d)** Total and $4f$ DOS at E_F . **(e)** Relaxation time τ ($\tau^{-1} = -2\text{Im}\Sigma$). **(f)** Imaginary part of the DMFT hybridization function at E_F .

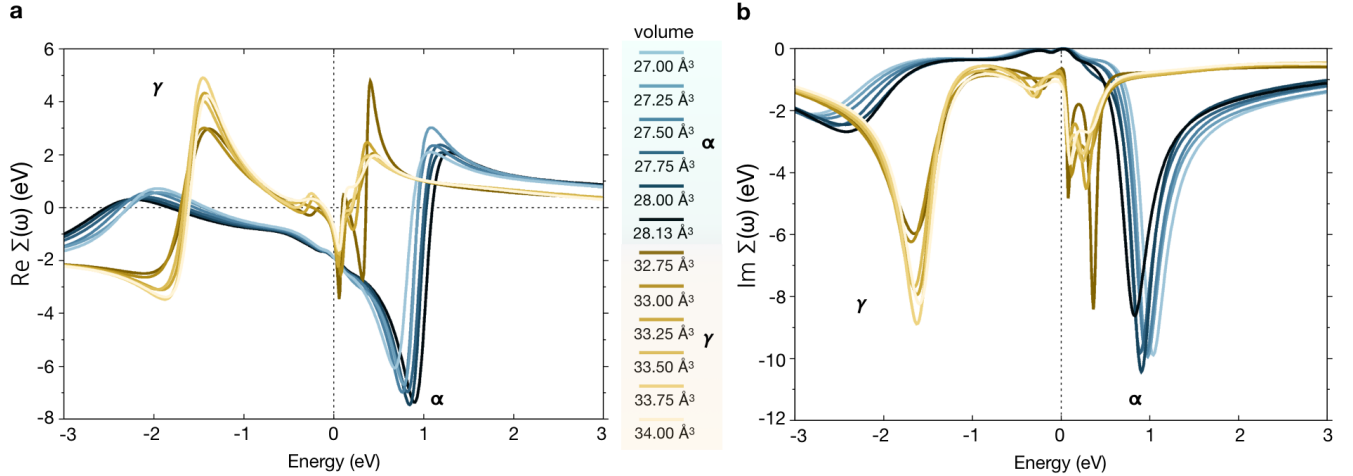


FIG. S4: (Color online) The self-energy $\Sigma(\omega)$ of single-particle Green's function of $4f_{j=5/2}$ orbital and its evolution in the pressure-volume isotherm ($T = 293\text{K}$) process. **(a)** The evolution of the real part of $\Sigma(\omega)$ for the γ - and α -phases. **(b)** The evolution of the imaginary part of $\Sigma(\omega)$ for the γ - and α -phases. Note the qualitatively different behaviors of self-energies between the two phases.

relaxation time τ is obtained from the inverse of the imaginary part of the self-energy Σ . The contribution of f electrons to the relaxation time is much bigger in α -Ce by two orders of magnitude. But, in reality, γ -phase has $5d$ band at E_F , and so the experimental relaxation times of both phases are comparable [21]. It is seen that $\text{Im}\Delta(0)$ increases by over 50 percent in average across the transition. This enhanced hybridization strength is one of the key ingredients that makes the system have non-trivial Z_2 topology. Figure S4 shows the self-energy $\Sigma(\omega)$ of $4f_{j=5/2}$ orbital and its evolution with respect to the pressure change. The self-energy obtained on the imaginary frequencies

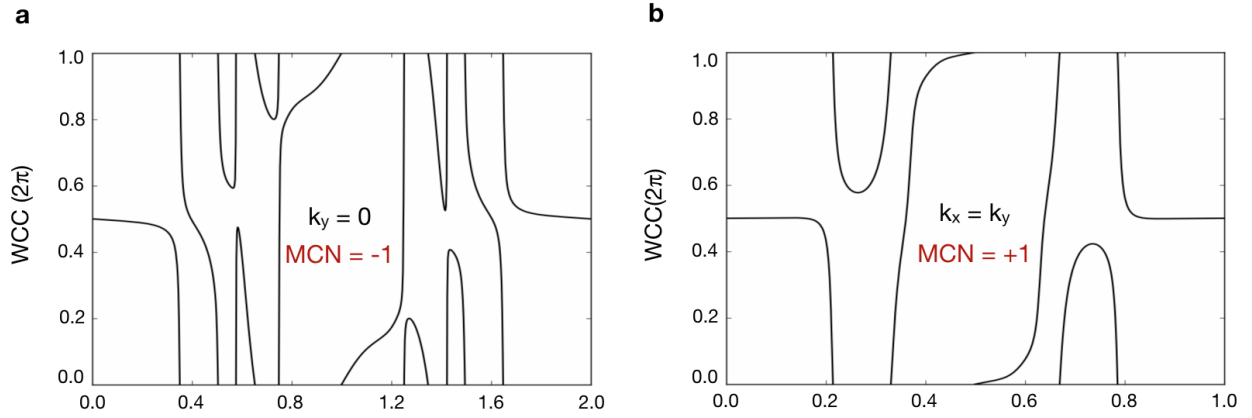


FIG. S5: The evolution of the Wannier charge center (WCC). Two distinct mirror Chern numbers (MCNs) for α -Ce are given along with the WCC evolutions. **(a)**, **(b)** MCNs for α -Ce: -1 for $k_y = 0$ planes, and $+1$ for $k_x = k_y$ planes, respectively. These MCNs correspond to those with mirror eigenvalue of $+i$ and are obtained from the Wilson-loop method.

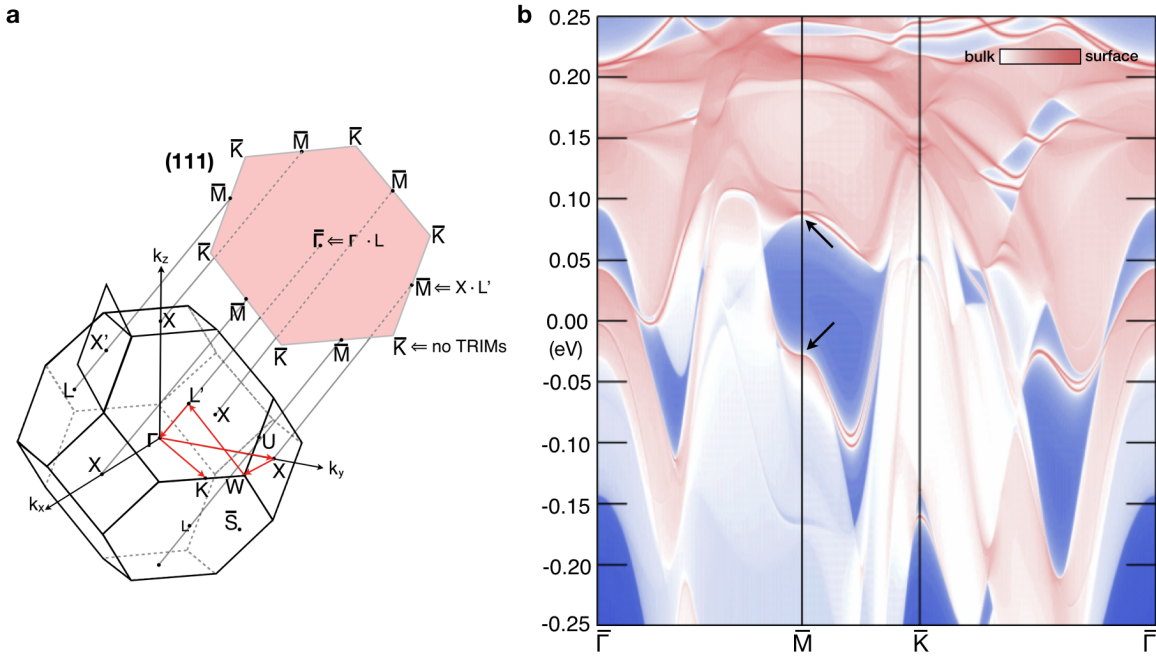


FIG. S6: (Color online) **(a)** Bulk and (111) surface BZ of fcc α -Ce. The TRIM point X in the bulk BZ is projected onto \bar{M} in the surface BZ. **(b)** The (111) surface electronic structure of α -Ce. It is calculated by a TB model with the semi-infinite slabs constructed from an effective topological Hamiltonian including Ce $6s$, $5p$, $d(t_{2g})$ and $4f_{5/2}$, $4f_{7/2}$ states based on the DFT result (rescaled by $1/2$ at around E_F). Two possible Dirac-cone candidates are indicated by two black arrows at \bar{M} .

are transformed into that on the real frequencies by using the maximum entropy method based on the analytic continuation. The qualitatively different behaviors of real and imaginary self-energies between the α and γ phases are remarkable, which produce quite distinct electronic structures between two.

V. TOPOLOGICAL CRYSTALLINE INSULATOR (TCI)-TYPE NATURE

Band inversion in combination with additional crystal symmetry can lead to another type of topological insulator (TI) nature, the so-called, topological crystalline insulator (TCI) nature. One of the simple crystal symmetries that is realized in real materials is the mirror symmetry. When Bloch states in a system are symmetric under the mirror operation, then, mirror Chern numbers (MCNs) are useful topological invariants to clarify the TI-type nature of materials. We have used the Wilson-loop method to calculate the MCNs of α -Ce. Figure S5 presents the MCN sets of the Bloch states on the corresponding mirror-symmetry planes with the mirror eigenvalue of $+i$ for α -Ce. The MCNs are obtained for the two mirror planes $k_y = 0$ and $k_x = k_y$. As shown in Fig. S5 α -Ce has the nontrivial MCNs of ($C_{k_y=0}^{+i} = -1$, $C_{k_x=k_y}^{+i} = +1$), which are the same as those of g-SmS [22]. This indicates that both systems would be TCI systems.

VI. SURFACE STATES AT (111) SURFACES

For the (111) surface Brillouin zone (BZ), one bulk X time-reversal invariant momentum (TRIM) point is projected onto \bar{M} . As shown in Fig. S6, in this case too, most surface states are buried under the bulk-projected bands. But Dirac cone-like bands are vaguely seen at around $+90$ meV and -30 meV at \bar{M} , as designated by black arrows.

-
- [S1] Haule, K. Yee, C.-H. and Kim, K. Dynamical mean-field theory within the full-potential methods: Electronic structure of CeIrIn₅, CeCoIn₅, and CeRhIn₅. *Phys. Rev. B* **81**, 195107 (2010).
- [S2] B. Blaha, K. Schwarz, G. K. H. Madsen, D. Kvasnicka, and J. Luitz, WIEN2k, An Augmented Plane Wave Plus Local Orbital Program for Calculating Crystal Properties (Vienna University of Technology, Austria, 2001).
- [S3] K. Haule, Quantum Monte Carlo impurity solver for cluster dynamical mean-field theory and electronic structure calculations with adjustable cluster base. *Phys. Rev. B* **75**, 155113 (2007).
- [S4] P. Sémon, C. Yee, K. Haule and A.-M. S. Tremblay Lazy skip-lists: An algorithm for fast hybridization-expansion quantum Monte Carlo. *Phys. Rev. B* **90**, 075149 (2014).
- [S5] K. Haule, C. Yee and K. Kim. Dynamical mean-field theory within the full-potential methods: Electronic structure of CeIrIn₅, CeCoIn₅, and CeRhIn₅. *Phys. Rev. B* **81**, 195107 (2010).
- [S6] K. Haule, T. Birol and G. Kotliar. Covalency in transition-metal oxides within all-electron dynamical mean-field theory. *Phys. Rev. B* **90**, 075136 (2014).
- [S7] A. A. Mostofi, J. R. Yates, Y.-S. Lee, I. Souza, D. Vanderbilt, and N. Marzari, Wannier90: A tool for obtaining maximally-localised Wannier functions. *Computer Physics Communications* **178**, 685 (2008).
- [S8] J. Kuneš, R. Arita, P. Wissgott, A. Toschi, H. Ikeda and K. Held, Wien2wannier: From linearized augmented plane waves to maximally localized Wannier functions. *Computer Physics Communications* **181**, 1888 (2010).
- [S9] N. Marzari, A. A. Mostofi, J. R. Yates, I. Souza and D. Vanderbilt, Maximally localized Wannier functions: Theory and applications. *Rev. Mod. Phys.* **84**, 1419 (2012).
- [S10] A. A. Mostofi, J. R. Yates, G. Pizzi, Y. S. Lee, I. Souza, D. Vanderbilt and N. Marzari, An updated version of wannier90: A tool for obtaining maximally-localised Wannier functions. *Comput. Phys. Commun.* **185**, 2309 (2014).
- [S11] M. P. Lopez Sancho and J. M. Lopez Sancho, Highly convergent schemes for the calculation of bulk and surface Green functions. *J. Phys. F : Met. Phys.* **15**, 851 (1985).
- [S12] Q. S. Wu, S. N. Zhang, H.-F. Song, M. Troyer and A. A. Soluyanov, WannierTools: An open-source software package for novel topological materials. *Comput. Phys. Commun.* **224**, 405 (2018).
- [S13] P. W. Bridgman, Rough Compressions of 177 Substances to 40,000 Kg/Cm³. *Proc. Am. Acad. Arts Sci.* **76** 71 (1948).
- [S14] A. W. Lawson, T- Y. Tang, *Phys. Rev.* **76** 301 (1949) Concerning the High Pressure Allotropic Modification of Cerium. *Phys. Rev.* **76** 301 (1949).
- [S15] M. J. Lipp, D. Jackson, H. Cynn, C. Aracne, W. J. Evans and A. K. McMahan Thermal Signatures of the Kondo Volume Collapse in Cerium. *Phys. Rev. Lett.* **101** 165703 (2008).
- [S16] L. H. Adams and B. L. Davis, Rapidly running transitions at high pressure. *Proc. Nat. Acad. Sci. US* **48** 982 (1962).
- [S17] B. J. Beaudry and P. E. Palmer, The lattice parameters of La, Ce, Pr, Nd, Sm, Eu and Yb. *J. Less-Common Metals* **34** 225 (1974).
- [S18] I. M. Lifshitz, Anomalies of electron characteristics of a metal in the high pressure region. *Sov. Phys. JETP* **11**, 1130 (1960).
- [S19] Hong Chul Choi, B. I. Min, J. H. Shim, K. Haule and G. Kotliar, Temperature-Dependent Fermi Surface Evolution in Heavy Fermion CeIrIn₅. *Phys. Rev. Lett.* **108**, 016402 (2012).
- [S20] C.-J. Kang, H. C. Choi, K. Kim, and B. I. Min, Topological Properties and the Dynamical Crossover from Mixed-Valence to Kondo-Lattice Behavior in the Golden Phase of SmS. *Phys. Rev. Lett.* **114**, 166404 (2015).

- [S21] J. W. van der Eb, A. B. Kuzmenko and D. van der Marel, Infrared and Optical Spectroscopy of α - and γ -Phase Cerium. *Phys. Rev. Lett.* **86**, 3407 (2001).
- [S22] C.-J. Kang *et al.* Unpublished (2019).